ACS OMEGA

Article

Cite This: ACS Omega 2018, 3, 9210−9219

http://pubs.acs.org/journal/acsodf

Multifunctional Nanosystem for Targeted and Controlled Delivery of Multiple Chemotherapeutic Agents for the Treatment of Drug-Resistant Breast Cancer

Song Lou, Zongmin Zhao, Micah Dezort, Taylor Lohneis, and Chenming Zhang*

Department of Biological Systems Engineering, Virginia Polytechnic Institute and State University, Blacksburg, Virginia 24061, United States

ABSTRACT: By targeting CD44 receptors, inhibiting multidrug resistance (MDR), controlling drug release, and synergistically inhibiting tumor growth, a multilayered nanosystem was developed to serve as a multifunctional platform for the treatment of drug-resistant breast cancers. The multilayer nanosystem is composed of a poly(lactic-*co*-glycolic acid) core, a liposome second layer, and a chitosan third layer. The chitosan-multilayered nanoparticles (Ch-MLNPs) can co-deliver three chemotherapeutic agents: doxorubicin (DOX), paclitaxel (PTX), and silybin. The three drugs are released from the multilayered NPs in a controlled and sequential manner upon internalization and localization in the cellular endosomes. The presence of a chitosan layer allows the nanosystem to target a well-characterized MDR breast cancer biomarker, the CD44s receptor. In vitro cytotoxicity study showed that the nanosystem loaded with triple drugs, DOX−PTX−silybin, resulted in better antitumor efficacy than the single-drug or dual-drug nano-formulations. Likely attributed to the MDR-inhibition effect of silybin, the co-delivered DOX and PTX exhibited a better synergistic effect on MDR breast cancer cells than on non-MDR breast cancer cells. The in vivo study also showed that the multilayered nanosystem promoted MDR inhibition and synergy between chemotherapeutic agents, leading to significant tumor reduction in a xenograft animal model. Ch-MLNPs reduced the tumor volume by fivefold compared to that of the control group without causing overt cytotoxicity.

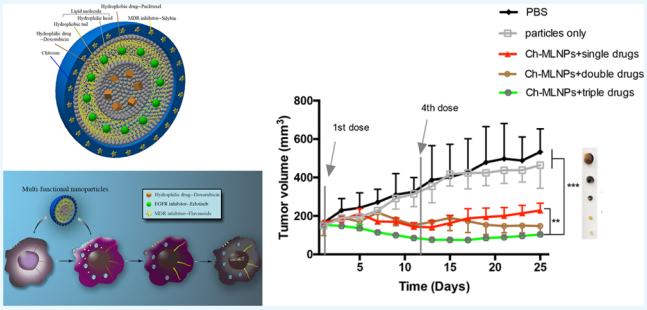

1. INTRODUCTION

In cancer therapy, the efficiency of delivering anticancer drugs to tumor sites via nanoparticles (NPs) is crucial. Much effort has been devoted to optimize NP delivery systems, and so far many systems have aimed to effectively deliver and release a single drug to treat various tumors.[1−8] However, single-drug systems are often inadequate in treating drug-resistant cancers.[9−14]

The key for using NP-mediated drug delivery systems to effectively inhibit cancer progression is to target multiple cancer pathways.[15,16] However, simultaneously delivering multiple drugs and inhibitors to target tumor sites and controlling the release of loaded chemotherapeutic drugs according to their unique mechanisms of action have remained a challenge.[17] Although traditional nanodelivery systems have been reported to be able to carry two drugs (or small interfering RNA),[18−20] studies on multi-agent-based cancer therapy, in which multiple mechanisms of action and synergistic inhibitions can be achieved, have been scarce. Ideally, an effective multi-agent-based cancer therapy should have a first agent that can sensitize the cancer cells and a second agent that would take advantage of the vulnerable state of cancer cells to enhance their cytotoxic efficacy.[15] In recent years, polymeric NPs, which are capable of delivering chemosensitizing agents to block the activity of P-glycoprotein (P-gp) or breast cancer resistance protein (BCRP) for multidrug resistance (MDR) in cancer cells, have attracted increased research interest.[21−24] Flavonoids, which are a class of pigments found in almost all plants and their products,[25] have shown strong inhibition of P-gp-mediated and BCRP-mediated efflux and thus can increase the cellular accumulation of P-gp and BCRP substrates and restore the sensitivity of MDR cells.[26−29] Previous studies have demonstrated that some flavonoids can be used alone to inhibit P-gp and reverse BCRP-mediated MDR even at very low concentrations (~50 μM).[30]

In this study, a new multilayered and multifunctional nanosystem, chitosan−liposome−poly(lactic-*co*-glycolic acid) (PLGA) NPs, was fabricated for efficient MDR inhibition, simultaneous delivery of multiple drugs, and controlled drug release for cancer therapy (Figure 1). The inclusion of the chitosan layer was based on the hypothesis that it could aid in tumor targeting.[1] The chitosan layer also provides a dynamic "cloud" to render the nanosystem "stealth," repelling plasma proteins and avoiding capture by macrophages.[31−34] Thus, the chitosan layer can prolong the half-life of the NPs in blood,

Received: May 9, 2018
Accepted: July 31, 2018
Published: August 15, 2018

DOI: 10.1021/acsomega.8b00949
ACS Omega 2018, 3, 9210−9219

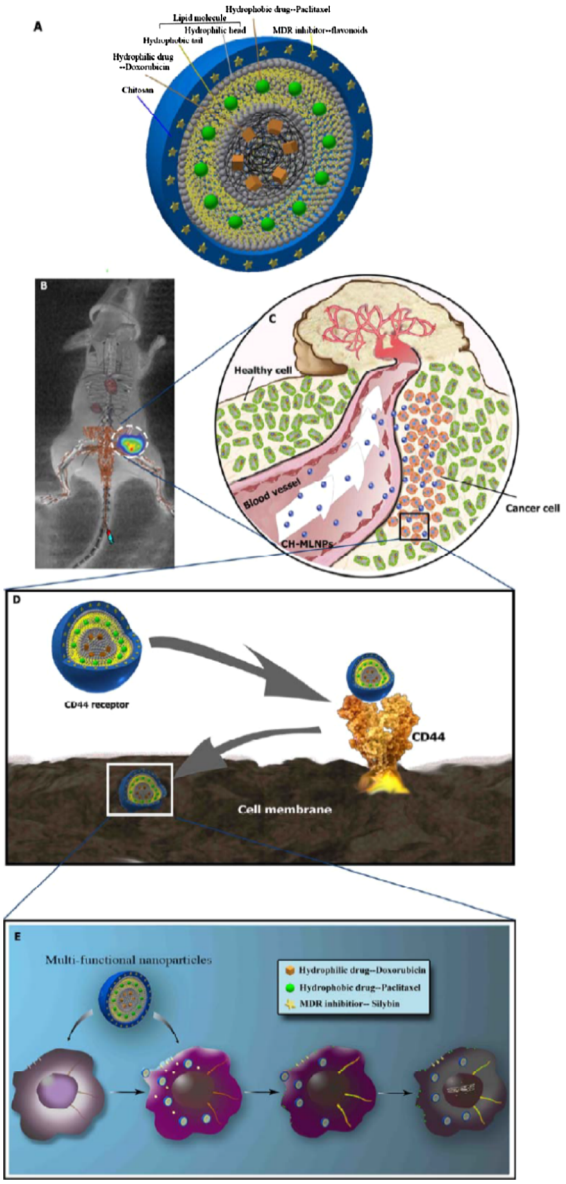

Figure 1. Illustration of the structure of the multilayered NPs and their functions. (A) Structure of Ch-MLNPs. (B) Schematic illustration of the transport of Ch-MLNPs in targeting tumors via: (C) EPR effect and (D) selective binding of Ch-MLNPs to CD44 receptors overexpressed on cancer cells. (E) The three loaded drugs (silybin, PTX, and DOX) are released at different time points and act on different targets in the cancer cell. Silybin is released first, followed by PTX, and finally DOX. This time-staggered effect is ideal for maximal efficacy of drug therapy. Inhibition of the MDR effect will maximize the effective drug content in cancer cells, and DOX can induce substantial DNA damage after PTX has sensitized the cancer cells.

reduce allergic reactions and rejection by immune clearance, and target cancer cells through selective binding to the CD44 receptors. The unique multilayered structure enables the loading of three chemotherapeutic agents into different layers to achieve controlled and sequential release. Silybin, a flavonoid that was encapsulated in the chitosan layer, can act as an MDR inhibitor by inhibiting the "drug-pumping" effect mediated by the P-gp pump.[35] Paclitaxel (PTX) and doxorubicin (DOX) were respectively loaded into the liposome and PLGA layer of the NPs, and they could act synergistically[36] to kill cancer cells by taking advantage of the vulnerable state of cancer cells caused by silybin.

2. RESULTS AND DISCUSSION

Chitosan-multi-layered NPs (Ch-MLNPs), consisting of three layers, were fabricated by first forming PLGA NPs, followed by assembling a double layer of lipids[37] and then a layer of chitosan.[38] DOX was encapsulated in PLGA through a double emulsion method. The DOX-loaded PLGA NPs were then encapsulated in 1,2-distearoyl-*sn*-glycero-3-phosphocholine (DSPC) liposomes, in which PTX was loaded via hydrophobic interactions between the drug and the hydrophobic tails of lipids. The resultant particles (liposome−PLGA) were then coated with a silybin-loaded chitosan layer. The structure of drug-loaded multilayered NPs was verified by dynamic light scattering, transmission electron microscopy (TEM), and confocal laser scanning microscopy (CLSM). The particle size and surface charge of the NPs gradually changed during the fabrication process. The NPs had a final ζ potential of 7.56 ± 0.54 mV and a diameter of 223 ± 73 nm (Figure 2A), which are favorable for the enhanced permeability and retention (EPR) effect.[39−42] TEM images (Figure 2B(a−c), right panels) confirmed the structure of the PLGA core, the liposome layer, and the outermost chitosan shell, respectively. The presence of the liposome and chitosan layers on the PLGA NPs was evident based on the increase in NP size with the low polydispersity index (PDI) after the addition of each layer (Figure 2B(a−c), left panels). As shown in Figure 2C, Ch-MLNPs were more stable in 0.01 M pH 7.4 phosphate buffered saline (PBS) than in 10% human serum. From the CLSM analyses (Figure 3A), co-localization of the three fluorescent colors [red from DOX-labeled PLGA, green from 1,2-dipalmitoyl-*sn*-glycero-3-phosphoethanolamine-*N*-(7-nitro-2-1,3-benzoxadiazol-4-yl) (NBD)-labeled liposome, and blue from Alexa Fluor 350-labeled chitosan] also confirmed the formation of a multilayered nanostructure. Figure 3B shows the zoomed-in confocal images, which clearly show that the three layers were assembled together to form Ch-MLNPs.

The loading of DOX into PLGA was analyzed by a fluorescence-based assay with excitation at 530 nm and emission at 590 nm,[43] whereas PTX and silybin loading were quantified using high-performance liquid chromatography (HPLC) monitored at 227 and 280 nm,[44,45] respectively. The multilayered NPs could load approximately 75 ± 10 μg/mg of DOX, 120 ± 12 μg/mg of PTX, and 90 ± 12 μg/mg of silybin. A drug-loading ratio of 3:5 (DOX/PTX) was selected according to our previous study[18] and published data on the synergistic effect between DOX and PTX.[46] The drug release profiles were determined by a dialysis method as reported elsewhere without the presence of serum.[47] According to the drug release profiles (Figure 4A), the MDR inhibitor, silybin, which was localized in the outermost layer, was released first, followed by PTX from the liposome layer and DOX from the PLGA core. Similarly, the line fittings and calculated EC50 also show the release tendency of each individual drug, with silybin released first, followed by PTX, and subsequently DOX. In contrast, the release profiles of DOX and PTX from control particles in which both drugs were loaded into the PLGA core, which was coated by drug-free liposome and chitosan layers, were almost identical (Figure 4B). The similar EC_{50} values of PTX and DOX, which were loaded in the same layer, also indicate there is no significant difference between the two release profiles. Compared with the reported drug release

DOI: 10.1021/acsomega.8b00949
ACS Omega 2018, 3, 9210−9219

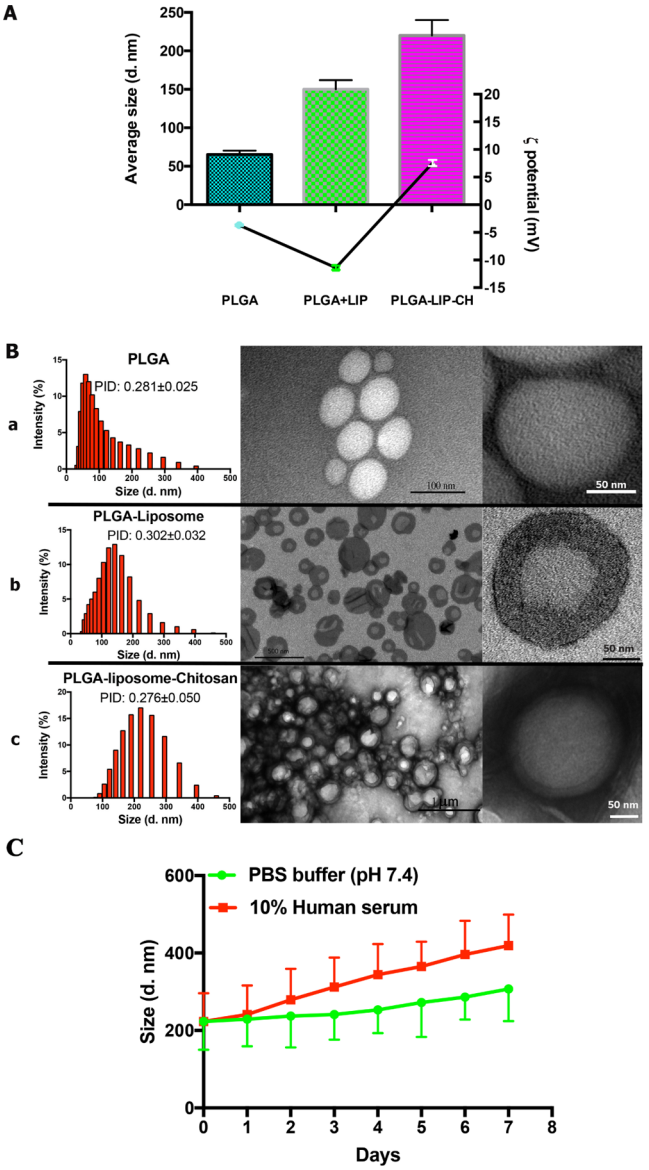

Figure 2. Structure of the multilayered NPs. (A) Hydrodynamic size and ζ potential and (B) morphological properties of MLNPs. TEM images (B, right panels) show the structure of PLGA NPs (panel a), PLGA−liposome NPs (panel b), and Ch-MLNPs (panel c). Dynamic light scattering results with PDI of the NPs at different fabrication stages (B, left panels). (C) Stability of Ch-MLNPs in different buffers.

profiles from PLGA particles,[48−50] the release of drugs enclosed in the PLGA core of the multilayered NPs was delayed by more than 10 h, revealing the effect of the liposome and chitosan layers.

For the three-layered NPs with DOX loaded, at 3 h, Ch-MLNPs were concentrated around the cell nuclei and a substantial amount of the multilayered NPs have been internalized into the cells (Figure 5A—3 h panel). Co-localization of the red (DOX) and green (NPs) fluorescence in cells indicated that the integrity of the multilayered NPs was still intact in the intracellular environment. After 3 h, indicated by the increased fluorescence intensity, more NPs were observed to accumulate in the cells as the incubation time increased. The NPs began to release DOX at 5 h post-incubation (5 h, DOX image), although the orange color in the merged image indicated that DOX had yet entered the cell nuclei (5 h, merged image). At 6 h, DOX was released from the NPs (6 h, DOX image) and began to enter the cell nuclei, as indicated by the arrows in the images. However, the boundary of nuclei is still not sharp, as shown in the enlarged image, indicating that a large proportion of the released DOX had not entered the cell nuclei. At 24 h post-incubation, the purple color (24 h, merged image) indicates that DOX had mostly been released from the NPs and entered the nuclei. The sharp nuclei boundary in the enlarged image shows distinctively that most of the loaded DOX had entered the cell nuclei.

Interestingly, in addition to their high capability to target overexpressed CD44 receptors on cancer cells, the multilayered NPs were also found to concentrate around the nuclei of cancer cells. This suggests that the multilayered NPs appear to accumulate around nuclei (Figure 5—3 h panel), agreeing with previously published results.[51,52] Meanwhile, the PLGA-only NPs, which served as a control, did not show any concentrated color around the nuclei as compared to the multilayered NPs (Figure 5A−B).

The in vitro antitumor efficacy of the chitosan- and non-chitosan NPs on MDR- and non-MDR cancer cells were compared (Figure 6). In the MDR cancer cells (Figure 6A), chitosan-coated NPs showed improved binding capacity over NPs without chitosan, as seen by the higher fluorescence intensity in Ch-MLNP-treated cells after 2 h of exposing the cells to respective NPs. Although the fluorescence intensity increased with culture time for both types of NPs, chitosan-coated NPs showed significantly improved binding capacity after 1 h. The p value increased with longer cultured time. On the other hand, for the non-MDR cancer cells (Figure 6B), chitosan-coated NPs did not show significantly improved binding capacity. The endocytosis mediated by the chitosan−CD44 interactions was the main mechanism for the uptake of chitosan-coated nanosystem.[1] Although to date, there is no report of higher binding capacity on MDR cells than on non-MDR cells for chitosan materials, this study proves the significant difference in binding capacity between chitosan-coated NPs and MDR and non-MDR cancer cells. Given the fact that the tested non-MDR cancer cell, A549,[53] does not express CD44s as the surface marker,[54] this observation suggests that the chitosan−CD44s interaction might be the main reason for the selective uptake. This mechanism was also supported by the conclusions of previous reports,[55,56] which showed CD44v was not present on MDR cancer cells, and the physical and genetic interaction between CD44s and P-gp is in part responsible for the MDR in cancer cells. This further indicates that CD44s might be the targeted binding protein for chitosan.

The in vitro antitumor efficacy of different drug formulations was tested using 3-(4,5-dimethylthiazol-2-yl)-2,5-diphenyltetrazolium bromide (MTT) assay in MDA-MB-231 and A-549 cancer cells. The viability of cancer cells treated with various doses (sum of all of the drugs) of drug formulations is shown in Figure 7A. As a P-gp pump inhibitor, silybin-loaded Ch-MLNPs (without DOX and PTX) showed little anticancer capacity, which agrees with the reported anticancer growth inhibitory effects of silybin.[57] In order to investigate the impacts of drug concentration on cell viability, the regulatory impact analysis (RIA) was used, which could provide a detailed and systematic appraisal of the potential impacts of drug concentration on cell viability.[58] The results (Figure 7B) indicate the drug-loaded Ch-MLNPs had a better anticancer

DOI: 10.1021/acsomega.8b00949
ACS Omega 2018, 3, 9210−9219

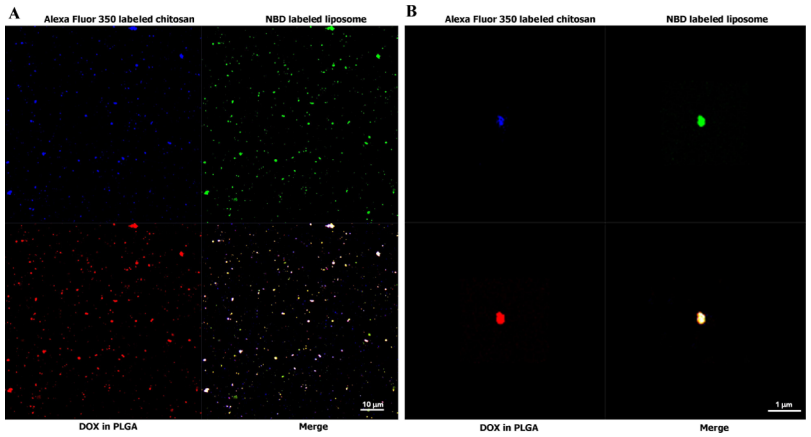

Figure 3. Confirmation of the multilayered structure of drug-loaded NPs. CLSM characterization of fluorescently labeled Ch-MLNPs, in which chitosan was covalently labeled with Alexa Fluor 350 (blue) and the liposome was labeled with NBD (green). DOX naturally fluoresces (red). (A) The zoom-out CLSM images of NPs. (B) The zoom-in CLSM images of NPs.

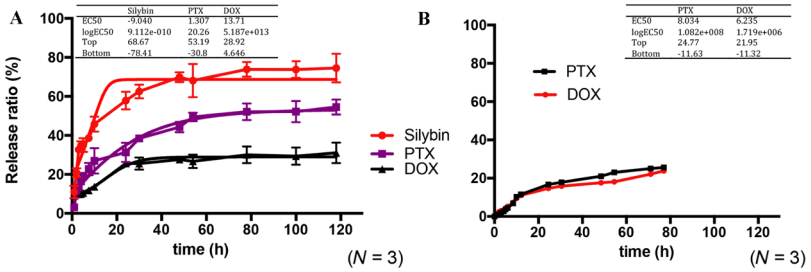

Figure 4. Drug release profiles of Ch-MLNPs in PBS and the respective release parameters evaluated from the slope and intercept of the three-parameter line fitting. (A) Drug release profiles of silybin, PTX, and DOX. (B) Drug release profiles of PTX and DOX, which were both loaded in the PLGA core of Ch-MLNPs. The EC_{50} is the concentration that gives a response half way between the bottom and top plateaus of the curve.

capacity on MDR cancer cells than on non-MDR cancer cells. Moreover, the triple-drug-loaded nanosystem performed better than the double-drug-loaded nanosystem (without silybin) on MDR cancer cells, likely because of the activity of silybin on blocking P-gp. The cytotoxicity efficacy of different formulations on MDR- and non-MDR cancer cells was compared (Figure 7C). For both cancer cells, the triple-drug-loaded and double-drug-loaded MLNPs had a better IC_{50} than DOX- or PTX-loaded MLNPs, especially on MDR cancer cells, demonstrating the benefit of the synergistic effect of these two or three drugs in the nano-formulations.

In order to study the synergistic effect among different drugs, combination indices (CI_{50}) were calculated.[59] CI_{50}, defined by the following equation, compares the required concentrations of multiple compounds administered in combination to that of a single agent compound required to give the same fractional effect. The modified CI_{50} equation is

$$CI_{50} = \frac{\frac{D_1 ComboIC_{50}}{D_1 IC_{50}} + \frac{D_2 ComboIC_{50}}{D_2 IC_{50}} + \cdots + \frac{D_n ComboIC_{50}}{D_n IC_{50}}}{n/2}$$

(n: the type number of loaded drug)

The equation calculates CI_{50} by adding the responses of the number of compounds administered and taking into consideration the ratio at which these more compounds are administered. When $CI_{50} = 1$, the effects of drugs are additive; when $CI_{50} < 1$, the combination is synergistic; when $CI_{50} > 1$, the combination is antagonistic.

As shown in Figure 7D, DOX−PTX−silybin MLNPs resulted in a better synergistic effect than DOX−PTX MLNPs on MDR cancer cells, as they had a significantly lower CI_{50}. Interestingly, the differences on the non-MDR cancer cells were not significant ($p > 0.05$). This discrepancy may be attributed to the MDR inhibition property of silybin, which can increase the anticancer efficiency of chemotherapeutic agents, DOX and PTX. For DOX−PTX−silybin MLNPs, there is no significant difference between MDR and non-MDR cancer cells, which indicates that the synergistic effect between DOX and PTX might be large enough to overshadow the effect between (DOX−PTX) and silybin.[60] Because the difference of DOX−PTX−silybin MLNPs between MDR and non-MDR is insignificant, the role of silybin in the synergistic effect was further studied by considering the DOX−PTX as one drug. The synergistic effect between silybin and (DOX−PTX) was identified by the IC_{50} of silybin MLNPs and DOX−PTX MLNPs (Figure 7E,F). Unlike the synergistic effect among the three drugs together, the role of silybin between MDR- and non-MDR cancer cells was significant. This significant difference suggested that the P-gp blocking property of silybin was applicable only to MDR cancer cells, rather than to the non-MDR cancer cells.

To evaluate the antitumor efficacy of the multilayered NPs in vivo, female BALB/c nude mice bearing subcutaneous xenograft tumors of MDA-MB-231 cells received intravenous administration of Ch-MLNPs. The controls included NPs loaded with DOX, with DOX and PTX, with PBS, and with empty particles without any drugs. The maximum tolerated dose (MTD) was first evaluated in a dose escalation study in

DOI: 10.1021/acsomega.8b00949
ACS Omega 2018, 3, 9210−9219

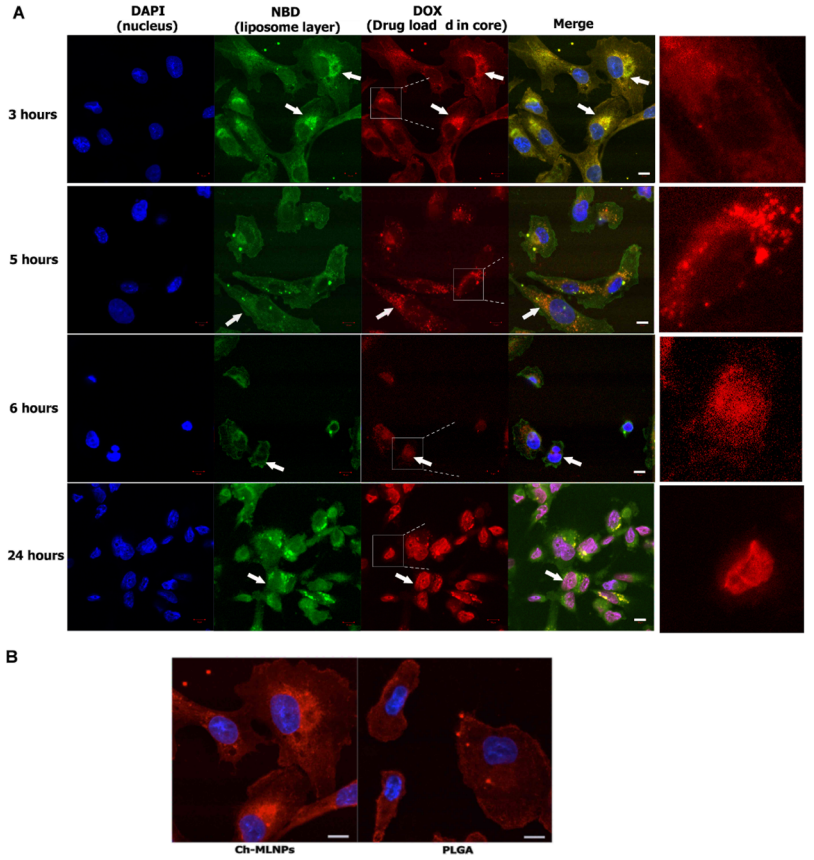

Figure 5. Confocal microscopic analysis of intracellular trafficking of Ch-MLNPs with DOX loaded in the core in MDA-MB-231 cells. (A) NP distribution at 3, 5, 6, and 24 h post-incubation. Nuclei were labeled with DAPI and liposomes were labeled with NBD (green). DOX, loaded in the core, is self-fluorescent (red). Arrows point to the intracellular tracking of NPs and loaded drugs at different culture times. (B) The intracellular distribution of Ch-MLNPs and PLGA in cancer cells (MDA-MB-231) after incubation for 3 h. Scale bar represents 10 μm.

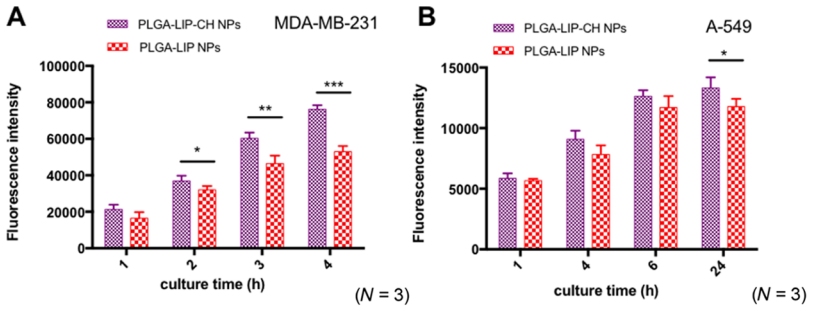

Figure 6. Cellular uptake of (A) MDA-MB-231 (MDR cancer cells) and (B) A-549 (non-MDR cancer cells) cells through flow cytometry after being exposed to different NP structures for various amount of time.

healthy female NCI nu/nu mice (6−8 weeks of age) through tail vein injection of 0.5, 1, 1.5, and 2.0 mg/kg of DOX encapsulated in multilayered NPs using a q4d × 4 regimen (once every four days for four doses with PBS as control). Results of survival study and body weight changes indicated that a dose of 2.0 mg/kg reduced mice weight by 15% and death ensued one day after the fourth dose. The MTD for all groups was determined to be 1.5 mg/kg of DOX under the 4 day dosing regimen. In the following in vivo efficacy test, mice were treated with DOX at the MTD through tail vein injection using a q4d × 4 regimen, and tumor volumes were monitored every 3 days. At the end point of the study (35th day), significant tumor regression was seen in the treatment group. The multilayered NPs (with three drugs) reduced the average tumor volume by 1.43- (n = 3, p = 0.07), 2.21- (n = 3, p < 0.01), 4.49-, and 5.115-fold (n = 3, p < 0.001) compared to the Ch-MLNP double-drug control, Ch-MLNP single-drug control, drug-free control, and PBS control, respectively (Figure 8A). Figure 8B shows the tumor shrinkage in the group treated with multilayered NPs in comparison with the group treated with PBS. In the particles-only treatment group, there is a small shrinking effect compared with the PBS controls, but it is not significantly different. This finding is in agreement with previous reports.[1] On the other hand, the statistical analysis shows an insignificant difference (p = 0.1363) of tumor shrinkage between DOX−PTX-loaded MLNPs (147.58 ± 40.62 mm^3) and DOX−PTX−silybin-loaded MLNPs (103.40 ± 6.50 mm^3), but it is worth pointing out that the animal

DOI: 10.1021/acsomega.8b00949
ACS Omega 2018, 3, 9210−9219

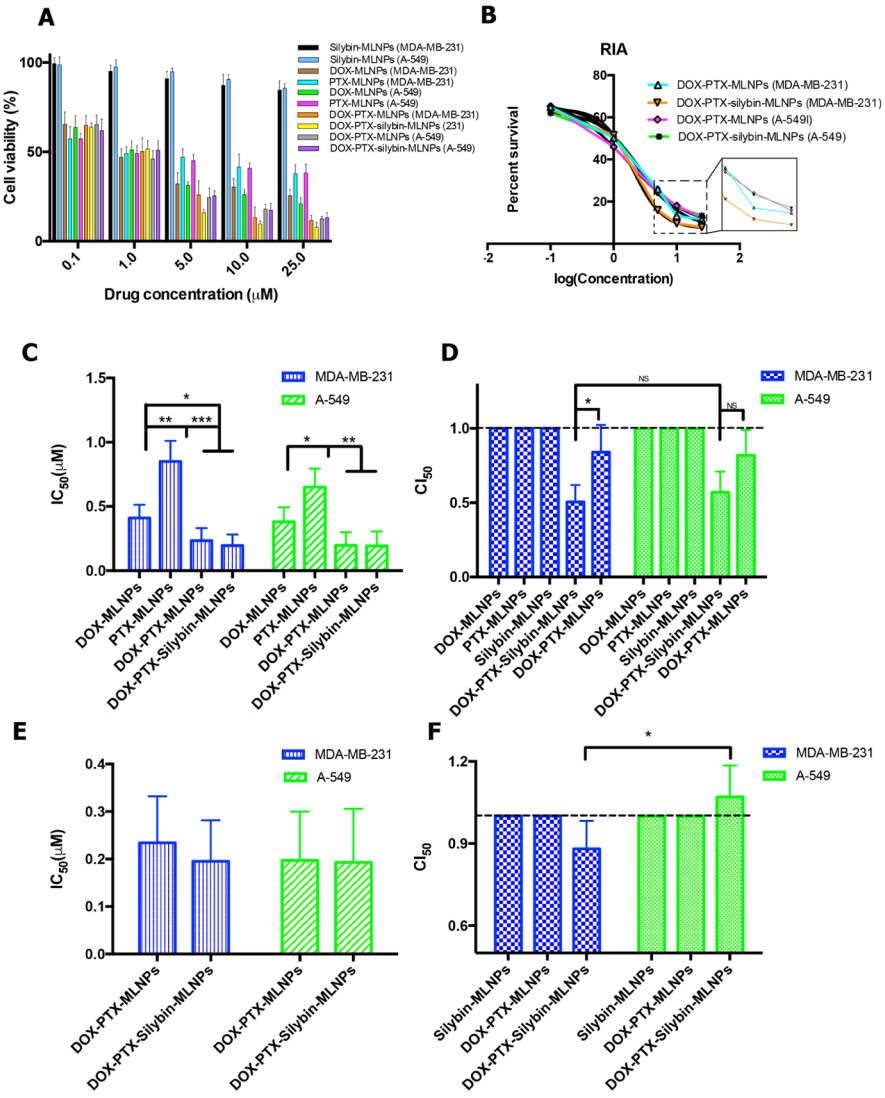

Figure 7. In vitro cytotoxicity of drug formulations in MDA-MB-231 breast cancer cells and A-549 lung cancer cells. (A) Cell viability of MDA-MB-231 and A-549 cells after being exposed to various doses of different drug formulations. (B) RIA of cell percent survival under various doses of different drugs. (C,D) IC_{50} (half maximal inhibitory concentration) and CI_{50} of different drug formulations exposed to MDA-MB-231 and A-549 cells. (E,F) IC_{50} and CI_{50} (between silybin and DOX−PTX) of dual-drug- and triple-drug-loaded Ch-MLNPs when exposed to MDA-MB-231 and A-549 cells. Comparison among groups was conducted by one-way ANOVA followed by Tukey's HSD analysis, $*p < 0.05$, $**p < 0.01$, $***p < 0.001$.

number is small in this study ($n = 3$). Nevertheless, an improved tumor shrinkage trend is still evident. There would be a significant difference in tumor shrinkage if N was increased to 8, but this was not feasible because of the constraints of this experiment. The results of mouse body weight change are shown in Figure 9A. No significant differences were found between the treatment group and the PBS control group. In addition, the histopathological analyses of mouse tissues collected at the end of the study (Figure 9B) show that treatment with Ch-MLNPs did not cause significant tissue damage, suggesting that Ch-MLNPs were not toxic at the MTD.

3. CONCLUSIONS

In this study, a three-layered nano-platform was developed that is capable of delivering multiple drugs. The nano-platform had a size of around 200 nm, which is relatively optimal for the EPR effects. Multiple drugs can be readily loaded and successfully delivered to tumors to counter the MDR effect. The nano-platform takes advantage of the interaction between chitosan and CD44s receptors, delayed drug release, and the synergistic effect among loaded drugs. Furthermore, the synergistic effects between the three loaded drugs were investigated on both MDR and non-MDR cancer cells through a modified CI_{50} model. Compared with the non-silybin formulation (DOX + PTX only), the silybin-loaded NPs (DOX + PTX + silybin) showed a significantly better result of P-gp blocking on MDR cancer cells, which enables an improved anti-tumor efficacy in vivo. This work demonstrated the potential of NPs as combination multi-therapeutic platforms for enhanced efficacy against drug-resistant breast cancer. With the unique transport process after cell uptake, it is possible to design NPs tailored for treating specific cancer patients with better clinical outcomes.

DOI: 10.1021/acsomega.8b00949
ACS Omega 2018, 3, 9210−9219

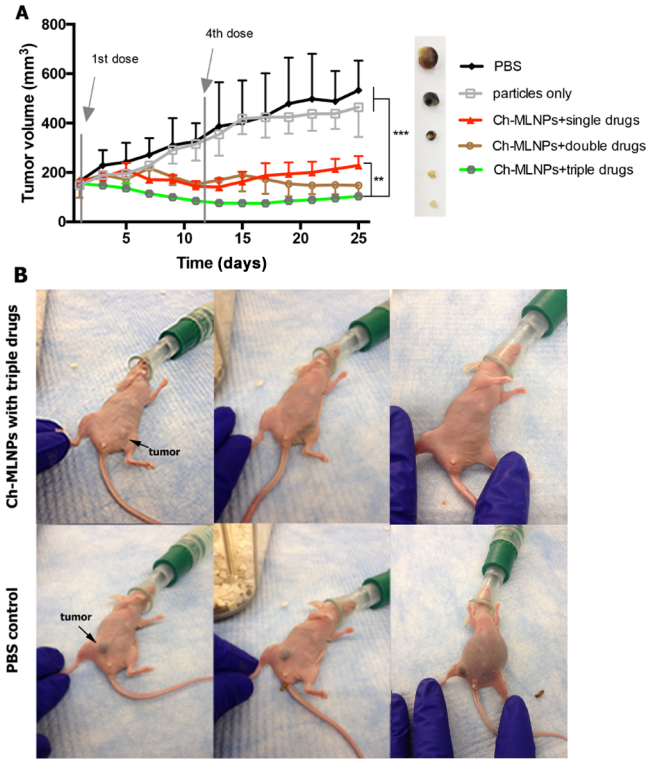

Figure 8. Efficacy of various drug formulations at MTDs in xenograft tumors. (A) Tumor growth inhibition of Ch-MLNPs with triple drug formulation as compared to Ch-MLNPs (particles only, no drug loaded), Ch-MLNPs with DOX (Ch-MLNPs + single drug), Ch-MLNPs with DOX and PTX (Ch-MLNPs + double drugs), as well as PBS. (B) The representative images of Ch-MLNP- and PBS-treated mice one day before the first dose, one day after the second dose, and at the end point of the study.

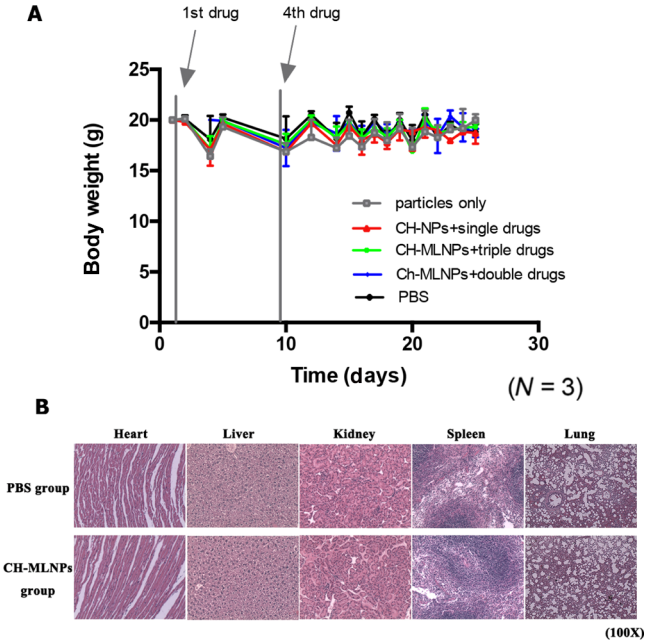

Figure 9. Preliminary toxicity study of Ch-MLNPs loaded with different drugs. (A) Body weight change for each animal treatment group. Signs of severe toxicity were not observed in any treatment group, although the animals in each group showed slight weight loss after the drug injections. The lost weight was regained in two weeks once the NP injection treatments had stopped. (B) Histology analysis of H&E-stained tissue sections isolated from mice of the treatment group (lower row of panels) and PBS-treated control group (upper row of panels).

4. MATERIALS AND METHODS

4.1. Materials. PLGA (Lactel 50:50, mol. weight 30 000−60 000) was purchased from Durect Corporation (Cupertino, CA). Chitosan (mol. weight 50 000−190 000) was purchased from Sigma-Aldrich (St. Louis, MO). DOX and PTX were ordered from LC Laboratories, Inc. (Woburn, MA, US). Coumarin-6, fluorescein isothiocyanate, dichloromethane (DCM), polyvinyl alcohol (PVA), and Nile red were purchased from Sigma-Aldrich, Inc. (Saint Louis, MO). Ready-to-use dialysis tubes [molecular weight cut-off (MWCO), 6000−8000] were purchased from Spectrum Laboratories, Inc. (Rancho Dominguez, CA, US). 4′,6-Diamidino-2-phenylindole (DAPI) and Alexa Fluor 350 were obtained from Life Technologies Corporation (Grand Island, NY, USA). Cancer cell lines (MDA-MB-231 and A-549) and related agents including trypsin/ethylenediamine tetraacetic acid solution, F-12K medium, L-15 medium, and fetal bovine serum were purchased from American Type Culture Collection (ATCC) (Manassas, VA, USA). All of the other chemicals were of analytical grade.

4.2. Preparation of Ch-MLNPs. The protocol for Ch-MLNPs preparation was developed based on a previously established method.[37,61] Briefly, PLGA was dissolved in DCM (20 mg/mL) and DOX was dissolved in distilled water (5 mg/200 μL). The DOX solution was then dropped into the PLGA solution and emulsified by sonication using a sonic dismembrator (model 500; Fisher Scientific, Pittsburg, PA, USA; operating frequency: 20 kHz) at 20% for 10 min. The resultant emulsion was added into 10 mL solution of PVA and was sonicated again at 70% for 90 s. Liposomes were formulated at a lipid mass ratio of 80:10:10 [DSPC/cholesterol/nitrobenzoxadiazole (NBD)]. These three components together with PTX (5 mg) were mixed well in chloroform and then desiccated to form a thin film through overnight vacuum drying. Liposome−PLGA NPs were prepared using a film-hydration−sonication method, as described previously.[62] One milliliter of 0.01 M pH 7.4 PBS was added to hydrate the lipid film. Then, the suspension was sonicated for 5 min in a Branson M2800H ultrasonic bath sonicator. Fifteen milligrams of PLGA NPs suspended in deionized water (10 mg/mL) were added into the above liposome suspension. Subsequently, in an ice−water bath, the mixture was sonicated using a bath sonicator for 5 min. Liposome−PLGA NPs were collected by centrifugation at 10 000*g* for 30 min. To prepare Ch-MLNPs, 2 mL liposome−PLGA was added dropwise to 30 mL chitosan solution that contains 10 mg of silybin, and the mixture was allowed to stir for 4 h.[63,64] Ch-MLNPs were washed with PBS three times and recovered by centrifugation at 7000*g* for 30 min.

4.3. Structural Characterization. Laser Doppler electrophoresis measurements were performed using a Malvern Nano-ZS Zetasizer (Malvern Instruments Ltd, Worcestershire, UK). The stability property of prepared NPs was investigated by measuring the change in NP size in 10% human serum (v/v) and 0.01 M PBS (pH 7.4) at room temperature under continuous stirring. The multilayered structure of the NPs was characterized by TEM (JEOL JEM 1400 instrument, JEOL Ltd., Japan) at a voltage of 120 kV and CLSM (Zeiss LSM 510 instrument, Carl Zeiss, Germany). A zetasizer test was completed using samples that were freshly prepared before

DOI: 10.1021/acsomega.8b00949
ACS Omega 2018, 3, 9210−9219

use by dispersing the NPs in ultrapure water. To image the NPs by negative TEM staining, the NPs were dissolved in 0.01 M of pH 7.4 PBS buffer and were negatively stained according to a standard procedure.[65] Fluorescent Ch-MLNPs were imaged by CLSM, in which the PLGA, liposome, and chitosan layers were labeled by DOX (red), NBD (green), and Alexa Fluor 350 (blue), respectively.

4.4. Release Kinetics of Drugs. A dialysis method was used to investigate in vitro release kinetics of drug-loaded NPs. In brief, 20 mg of drug-loaded NPs was dissolved in PBS with 0.1% (v/v) Tween 80, and dialyzed against 20 mL of that same buffer using ready-to-use dialysis tubes (MWCO 6000−8000) under continuous stirring at 37 °C. At predetermined time points, 1 mL of the sample solution was taken out and an equal 1 mL fresh buffer was added. The concentrations of the drug were determined by measuring the fluorescence intensity for DOX[66] and HPLC for PTX[67] and silybin.[68]

4.5. In Vitro Experiments. *4.5.1. Cell Culture.* Triple negative breast cancer cell line, MDA-MB-231, was obtained from ATCC (Manassas, VA). Cells were subcultured in the supplier's recommended basal medium supplemented with 10% fetal bovine serum, 50 units/mL of penicillin, and 50 units/mL of streptomycin in a humidified atmosphere. All experiments were performed on cells cultured 12−24 h before experimentation.

4.5.2. Cellular Uptake and Intracellular Distribution. The protocols for cellular uptake and intracellular distribution assays followed our previously published work.[47,69] For the intracellular distribution study, MDA-MB-231 cells were seeded onto a two-well chamber slide (Thermo Fisher Scientific Inc., Pittsburgh, PA) at a concentration of 2×10^5/chamber in 2 mL of medium and cultured overnight. The original medium was replaced with fresh medium (2 mL) containing 20 μg of Ch-MLNPs. Cells were incubated for 3, 5, 6, or 24 h. The nuclei of cells were labeled by DAPI, a dihydrochloride. Cells were imaged by CLSM. For the cellular uptake assays, the cells were seeded in a 12-well plate at a density of 5000 cells/well and treated with 50 μg of fluorescently labeled NPs for various periods of time at 37 °C, followed by washing and treating with trypsin. The cell-associated fluorescence was analyzed by a flow cytometer (BD FACSAria I, BD, Franklin Lakes, NJ) coupled with a high-throughput system.

4.5.3. In Vitro Cytotoxicity Assays. In vitro cytotoxicity of Ch-MLNPs was evaluated using a MTT assay following a protocol outlined elsewhere.[18] Briefly, cells were seeded at a density of 5000 cells/cell onto 96-well plates and incubated for 24 h. After replacing the original media with fresh media, cells were treated with different concentrations of drug formulations and incubated for 72 h. After replacing the media with fresh media containing MTT (0.5 mg/mL), cells were incubated for another 4 h at 37 °C. The media were then immediately removed, and 100 μL of dimethyl sulfoxide was added to solubilize the formazan crystals. Absorbance was measured at 570 nm through a Synergy HT Multi-Mode Microplate Reader (BioTek Instruments, Inc., Winooski, VT). Untreated cells were used as control to calculate cell viability.

4.6. In Vivo Experiments. Female nude mice (4−6 weeks old) were purchased from Charles River. All in vivo experiments were carried out under the supervision of the Institutional Animal Care and Use Committee (IACUC) of Virginia Tech. The tumor shrinkage efficacy of Ch-MLNPs was evaluated in a xenograft breast cancer model. In brief, 5×10^7 cells/mL MDA-MB-231 cells (0.1 mL) (50:50 mixed with BD Matrigel Basement Membrane Matrix) were injected subcutaneously into the hind flanks of 8-week-old BALB/c nude mice. Tumors were allowed to form for 2−3 weeks. When the tumor reached a volume of 100 mm^3, NP treatments were performed by intravenously administering NPs at the MTD via tail vein. Perpendicular tumor diameters were measured by digital caliper and used to calculate tumor volume according to the reported protocol every two days.[70,71] Mice were sacrificed when the tumors reached a volume of 600 mm^3.

4.7. Statistical Analysis. Data were expressed as mean ± standard deviation. Among multiple groups, significance tests were conducted using one-way analysis of variance (ANOVA) followed by Tukey's honest significant difference (HSD) analysis. Differences were considered as significant at p values < 0.05 (*), <0.01 (**), and <0.001 (***).

AUTHOR INFORMATION

Corresponding Author

*E-mail: chzhang2@vt.edu. Phone: +1-(540)231-7601. Fax: +1-(540)231-3199.

ORCID

Zongmin Zhao: 0000-0001-8979-844X

Chenming Zhang: 0000-0002-6770-5334

Notes

The authors declare no competing financial interest.

ACKNOWLEDGMENTS

This study was financially supported by the National Institute on Drug Abuse (U01DA036850) and the endowment fund of Elizabeth and James E. Turner Jr. '56 Faculty Fellow in Engineering at Virginia Tech.

REFERENCES

(1) Rao, W.; Wang, H.; Han, J.; Zhao, S.; Dumbleton, J.; Agarwal, P.; Zhang, W.; Zhao, G.; Yu, J.; Zynger, D. L.; Lu, X.; He, X. Chitosan-Decorated Doxorubicin-Encapsulated Nanoparticle Targets and Eliminates Tumor Reinitiating Cancer Stem-like Cells. *ACS Nano* **2015**, *9*, 5725−5740.

(2) Saha, A.; Mohanta, S. C.; Deka, K.; Deb, P.; Devi, P. S. Surface-Engineered Multifunctional Eu:Gd2O3 Nanoplates for Targeted and pH-Responsive Drug Delivery and Imaging Applications. *ACS Appl. Mater. Interfaces* **2017**, *9*, 4126−4141.

(3) Yan, X.; Yu, Q.; Guo, L.; Guo, W.; Guan, S.; Tang, H.; Lin, S.; Gan, Z. Positively Charged Combinatory Drug Delivery Systems against Multi-Drug-Resistant Breast Cancer: Beyond the Drug Combination. *ACS Appl. Mater. Interfaces* **2017**, *9*, 6804−6815.

(4) Deshpande, S.; Sharma, S.; Koul, V.; Singh, N. Core-Shell Nanoparticles as an Efficient, Sustained, and Triggered Drug-Delivery System. *ACS Omega* **2017**, *2*, 6455−6463.

(5) Galbis, E.; Iglesias, N.; Lucas, R.; Tinajero-Díaz, E.; de-Paz, M.-V.; Muñoz-Guerra, S.; Galbis, J. A. Validation of Smart Nanoparticles as Controlled Drug Delivery Systems: Loading and pH-Dependent Release of Pilocarpine. *ACS Omega* **2018**, *3*, 375−382.

(6) Pandit, G.; Roy, K.; Agarwal, U.; Chatterjee, S. Self-Assembly Mechanism of a Peptide-Based Drug Delivery Vehicle. *ACS Omega* **2018**, *3*, 3143−3155.

(7) Ou, Y.-C.; Webb, J. A.; Faley, S.; Shae, D.; Talbert, E. M.; Lin, S.; Cutright, C. C.; Wilson, J. T.; Bellan, L. M.; Bardhan, R. Gold Nanoantenna-Mediated Photothermal Drug Delivery from Thermosensitive Liposomes in Breast Cancer. *ACS Omega* **2016**, *1*, 234−243.

(8) Bagchi, D.; Dutta, S.; Singh, P.; Chaudhuri, S.; Pal, S. K. Essential Dynamics of an Effective Phototherapeutic Drug in a Nanoscopic Delivery Vehicle: Psoralen in Ethosomes for Biofilm Treatment. *ACS Omega* **2017**, *2*, 1850−1857.

DOI: 10.1021/acsomega.8b00949
ACS Omega 2018, 3, 9210−9219

(9) Cunha-Reis, C.; Machado, A.; Barreiros, L.; Araújo, F.; Nunes, R.; Seabra, V.; Ferreira, D.; Segundo, M. A.; Sarmento, B. Nanoparticles-in-film for the combined vaginal delivery of anti-HIV microbicide drugs. *J. Controlled Release* **2016**, *243*, 43−53.
(10) Chen, A. M.; Zhang, M.; Wei, D.; Stueber, D.; Taratula, O.; Minko, T.; He, H. Co-delivery of doxorubicin and Bcl-2 siRNA by mesoporous silica nanoparticles enhances the efficacy of chemotherapy in multidrug-resistant cancer cells. *Small* **2009**, *5*, 2673−2677.
(11) Huang, C.-C.; Huang, W.; Yeh, C.-S. Shell-by-shell synthesis of multi-shelled mesoporous silica nanospheres for optical imaging and drug delivery. *Biomaterials* **2011**, *32*, 556−564.
(12) Zhu, H.; Chen, H.; Zeng, X.; Wang, Z.; Zhang, X.; Wu, Y.; Gao, Y.; Zhang, J.; Liu, K.; Liu, R.; Cai, L.; Mei, L.; Feng, S.-S. Co-delivery of chemotherapeutic drugs with vitamin E TPGS by porous PLGA nanoparticles for enhanced chemotherapy against multi-drug resistance. *Biomaterials* **2014**, *35*, 2391−2400.
(13) Nguyen, C. T. H.; Webb, R. I.; Lambert, L. K.; Strounina, E.; Lee, E. C.; Parat, M.-O.; McGuckin, M. A.; Popat, A.; Cabot, P. J.; Ross, B. P. Bifunctional Succinylated ε-Polylysine-Coated Mesoporous Silica Nanoparticles for pH-Responsive and Intracellular Drug Delivery Targeting the Colon. *ACS Appl. Mater. Interfaces* **2017**, *9*, 9470−9483.
(14) Wang, L.; Zhang, P.; Shi, J.; Hao, Y.; Meng, D.; Zhao, Y.; Yanyan, Y.; Li, D.; Chang, J.; Zhang, Z. Radiofrequency-triggered tumor-targeting delivery system for theranostics application. *ACS Appl. Mater. Interfaces* **2015**, *7*, 5736−5747.
(15) Morton, S. W.; Lee, M. J.; Deng, Z. J.; Dreaden, E. C.; Siouve, E.; Shopsowitz, K. E.; Shah, N. J.; Yaffe, M. B.; Hammond, P. T. A Nanoparticle-Based Combination Chemotherapy Delivery System for Enhanced Tumor Killing by Dynamic Rewiring of Signaling Pathways. *Sci. Signal.* **2014**, *7*, ra44.
(16) Zhu, L.; Dong, D.; Yu, Z.-L.; Zhao, Y.-F.; Pang, D.-W.; Zhang, Z.-L. Folate-Engineered Microvesicles for Enhanced Target and Synergistic Therapy toward Breast Cancer. *ACS Appl. Mater. Interfaces* **2017**, *9*, 5100−5108.
(17) Koziolová, E.; Janoušková, O.; Cuchalová, L.; Hvězdová, Z.; Hraběta, J.; Eckschlager, T.; Sivák, L.; Ulbrich, K.; Etrych, T.; Šubr, V. Overcoming multidrug resistance in Dox-resistant neuroblastoma cell lines via treatment with HPMA copolymer conjugates containing anthracyclines and P-gp inhibitors. *J. Controlled Release* **2016**, *233*, 136−146.
(18) Zhao, Z.; Lou, S.; Hu, Y.; Zhu, J.; Zhang, C. A Nano-in-Nano Polymer-Dendrimer Nanoparticle-Based Nanosystem for Controlled Multidrug Delivery. *Mol. Pharm.* **2017**, *14*, 2697−2710.
(19) Yang, Q.; Li, L.; Sun, W.; Zhou, Z.; Huang, Y. Dual Stimuli-Responsive Hybrid Polymeric Nanoparticles Self-Assembled from POSS-Based Starlike Copolymer-Drug Conjugates for Efficient Intracellular Delivery of Hydrophobic Drugs. *ACS Appl. Mater. Interfaces* **2016**, *8*, 13251−13261.
(20) Shanmugam, V.; Chien, Y.-H.; Cheng, Y.-S.; Liu, T.-Y.; Huang, C.-C.; Su, C.-H.; Chen, Y.-S.; Kumar, U.; Hsu, H.-F.; Yeh, C.-S. Oligonucleotides-Assembled Au Nanorod-Assisted Cancer Photothermal Ablation and Combination Chemotherapy with Targeted Dual-Drug Delivery of Doxorubicin and Cisplatin Prodrug. *ACS Appl. Mater. Interfaces* **2014**, *6*, 4382−4393.
(21) Hu, C.-M. J.; Zhang, L. Nanoparticle-based combination therapy toward overcoming drug resistance in cancer. *Biochem. Pharmacol.* **2012**, *83*, 1104−1111.
(22) Dai, Z.; Yao, Q.; Zhu, L. MMP2-Sensitive PEG-Lipid Copolymers: A New Type of Tumor-Targeted P-Glycoprotein Inhibitor. *ACS Appl. Mater. Interfaces* **2016**, *8*, 12661−12673.
(23) Li, H.; Liu, C.; Zeng, Y.-P.; Hao, Y.-H.; Huang, J.-W.; Yang, Z.-Y.; Li, R. Nanoceria-Mediated Drug Delivery for Targeted Photodynamic Therapy on Drug-Resistant Breast Cancer. *ACS Appl. Mater. Interfaces* **2016**, *8*, 31510−31523.
(24) Zhang, Y.; Zhang, C.; Chen, J.; Liu, L.; Hu, M.; Li, J.; Bi, H. Trackable Mitochondria-Targeting Nanomicellar Loaded with Doxorubicin for Overcoming Drug Resistance. *ACS Appl. Mater. Interfaces* **2017**, *9*, 25152−25163.
(25) Kuhnau, J. The flavonoids. A class of semi-essential food components: their role in human nutrition. *World Rev. Nutr. Diet.* **1976**, *24*, 117−191.
(26) Jonker, J. W.; Buitelaar, M.; Wagenaar, E.; van der Valk, M. A.; Scheffer, G. L.; Scheper, R. J.; Plosch, T.; Kuipers, F.; Elferink, R. P. J. O.; Rosing, H.; Beijnen, J. H.; Schinkel, A. H. Nonlinear partial differential equations and applications: The breast cancer resistance protein protects against a major chlorophyll-derived dietary phototoxin and protoporphyria. *Proc. Natl. Acad. Sci. U.S.A.* **2002**, *99*, 15649−15654.
(27) Jonker, J. W.; Smit, J. W.; Brinkhuis, R. F.; Maliepaard, M.; Beijnen, J. H.; Schellens, J. H.; Schinkel, A. H. Role of breast cancer resistance protein in the bioavailability and fetal penetration of topotecan. *J. Natl. Cancer Inst.* **2000**, *92*, 1651−1656.
(28) Collnot, E.-M.; Baldes, C.; Wempe, M. F.; Hyatt, J.; Navarro, L.; Edgar, K. J.; Schaefer, U. F.; Lehr, C.-M. Influence of vitamin E TPGS poly(ethylene glycol) chain length on apical efflux transporters in Caco-2 cell monolayers. *J. Controlled Release* **2006**, *111*, 35−40.
(29) Agüeros, M.; Zabaleta, V.; Espuelas, S.; Campanero, M. A.; Irache, J. M. Increased oral bioavailability of paclitaxel by its encapsulation through complex formation with cyclodextrins in poly(anhydride) nanoparticles. *J. Controlled Release* **2010**, *145*, 2−8.
(30) Zhang, S.; Yang, X.; Morris, M. E. Flavonoids are inhibitors of breast cancer resistance protein (ABCG2)-mediated transport. *Mol. Pharmacol.* **2004**, *65*, 1208−1216.
(31) Bao, X.; Wang, W.; Wang, C.; Wang, Y.; Zhou, J.; Ding, Y.; Wang, X.; Jin, Y. A chitosan-graft-PEI-candesartan conjugate for targeted co-delivery of drug and gene in anti-angiogenesis cancer therapy. *Biomaterials* **2014**, *35*, 8450−8466.
(32) Mansur, A. A. P.; Mansur, H. S.; Soriano-Araújo, A.; Lobato, Z. I. P. Fluorescent nanohybrids based on quantum dot-chitosan-antibody as potential cancer biomarkers. *ACS Appl. Mater. Interfaces* **2014**, *6*, 11403−11412.
(33) Sanpui, P.; Chattopadhyay, A.; Ghosh, S. S. Induction of Apoptosis in Cancer Cells at Low Silver Nanoparticle Concentrations using Chitosan Nanocarrier. *ACS Appl. Mater. Interfaces* **2011**, *3*, 218−228.
(34) Yang, J.; Wu, Y.; Shen, Y.; Zhou, C.; Li, Y.-F.; He, R.-R.; Liu, M. Enhanced Therapeutic Efficacy of Doxorubicin for Breast Cancer Using Chitosan Oligosaccharide-Modified Halloysite Nanotubes. *ACS Appl. Mater. Interfaces* **2016**, *8*, 26578−26590.
(35) Maitrejean, M.; Comte, G.; Barron, D.; El Kirat, K.; Conseil, G.; Di Pietro, A. The flavanolignan silybin and its hemisynthetic derivatives, a novel series of potential modulators of P-glycoprotein. *Bioorg. Med. Chem. Lett.* **2000**, *10*, 157−160.
(36) Blagosklonny, M. V. Matching targets for selective cancer therapy. *Drug Discovery Today* **2003**, *8*, 1104−1107.
(37) Hu, Y.; Ehrich, M.; Fuhrman, K.; Zhang, C. In vitro performance of lipid-PLGA hybrid nanoparticles as an antigen delivery system: lipid composition matters. *Nanoscale Res. Lett.* **2014**, *9*, 434.
(38) Zhu, L.; Ma, J.; Jia, N.; Zhao, Y.; Shen, H. Chitosan-coated magnetic nanoparticles as carriers of 5-Fluorouracil: Preparation, characterization and cytotoxicity studies. *Colloids Surf., B* **2009**, *68*, 1−6.
(39) Kobayashi, H.; Watanabe, R.; Choyke, P. L. Improving Conventional Enhanced Permeability and Retention (EPR) Effects; What Is the Appropriate Target? *Theranostics* **2014**, *4*, 81−89.
(40) Wong, A. D.; Ye, M.; Ulmschneider, M. B.; Searson, P. C. Quantitative Analysis of the Enhanced Permeation and Retention (EPR) Effect. *PLoS One* **2015**, *10*, No. e0123461.
(41) Petros, R. A.; DeSimone, J. M. Strategies in the design of nanoparticles for therapeutic applications. *Nat. Rev. Drug Discovery* **2010**, *9*, 615−627.
(42) Blanco, E.; Shen, H.; Ferrari, M. Principles of nanoparticle design for overcoming biological barriers to drug delivery. *Nat. Biotechnol.* **2015**, *33*, 941−951.
(43) de Lange, J. H. M.; Schuurhuis, G. J.; ten Kate, T. K.; Van Heijningen, T. H. M.; Lankelma, J.; Baak, J. P. A. Quantification by

DOI: 10.1021/acsomega.8b00949
ACS Omega 2018, 3, 9210−9219

laser scan microscopy of intracellular doxorubicin distribution. *Cytometry* **1992**, *13*, 571−576.
(44) Jain, A.; Gulbake, A.; Jain, A.; Shilpi, S.; Hurkat, P.; Kashaw, S.; Jain, S. K. Development and validation of the HPLC method for simultaneous estimation of Paclitaxel and topotecan. *J. Chromatogr. Sci.* **2014**, *52*, 697−703.
(45) Cai, X.-L.; Li, D.-N.; Qiao, J.-Q.; Lian, H.-Z.; Wang, S.-K. Determination of Silymarin Flavonoids by HPLC and LC-MS and Investigation of Extraction Rate of Silymarin in Silybum marianum Fruits by Boiling Water. *Asian J. Chem.* **2009**, *21*, 63−74.
(46) Huang, Y.; Liu, W.; Gao, F.; Fang, X.; Chen, Y. c(RGDyK)-decorated Pluronic micelles for enhanced doxorubicin and paclitaxel delivery to brain glioma. *Int. J. Nanomed.* **2016**, *11*, 1629−1641.
(47) Huang, W.; Zhang, J.; Dorn, H. C.; Zhang, C. Assembly of Bio-Nanoparticles for Double Controlled Drug Release. *PLoS One* **2013**, *8*, No. e74679.
(48) Musumeci, T.; Ventura, C. A.; Giannone, I.; Ruozi, B.; Montenegro, L.; Pignatello, R.; Puglisi, G. PLA/PLGA nanoparticles for sustained release of docetaxel. *Int. J. Pharm.* **2006**, *325*, 172−179.
(49) Mu, L.; Feng, S. S. A novel controlled release formulation for the anticancer drug paclitaxel (Taxol): PLGA nanoparticles containing vitamin E TPGS. *J. Controlled Release* **2003**, *86*, 33−48.
(50) Mainardes, R. M.; Evangelista, R. C. PLGA nanoparticles containing praziquantel: effect of formulation variables on size distribution. *Int. J. Pharm.* **2005**, *290*, 137−144.
(51) Neubrand, V. E.; Will, R. D.; Möbius, W.; Poustka, A.; Wiemann, S.; Schu, P.; Dotti, C. G.; Pepperkok, R.; Simpson, J. C. γ-BAR, a novel AP-1-interacting protein involved in post-Golgi trafficking. *EMBO J.* **2005**, *24*, 1122−1133.
(52) Starkuviene, V.; Liebel, U.; Simpson, J. C.; Erfle, H.; Poustka, A.; Wiemann, S.; Pepperkok, R. High-content screening microscopy identifies novel proteins with a putative role in secretory membrane traffic. *Genome Res.* **2004**, *14*, 1948−1956.
(53) Wang, W.; Liu, X.; Tang, C. The difference between multi-drug resistant cell line A549/Gem and its parental cell A549. *Chin.-Ger. J. Clin. Oncol.* **2009**, *8*, 190−194.
(54) Leung, E. L.-H.; Fiscus, R. R.; Tung, J. W.; Tin, V. P.-C.; Cheng, L. C.; Sihoe, A. D.-L.; Fink, L. M.; Ma, Y.; Wong, M. P. Non-Small Cell Lung Cancer Cells Expressing CD44 Are Enriched for Stem Cell-Like Properties. *PLoS One* **2010**, *5*, No. e14062.
(55) Miletti-González, K. E.; Chen, S.; Muthukumaran, N.; Saglimbeni, G. N.; Wu, X.; Yang, J.; Apolito, K.; Shih, W. J.; Hait, W. N.; Rodríguez-Rodríguez, L. The CD44 receptor interacts with P-glycoprotein to promote cell migration and invasion in cancer. *Cancer Res.* **2005**, *65*, 6660−6667.
(56) Wang, W.; Liu, X.; Liu, G.; Tang, C.; Qu, L.; Wang, W. The difference between multi-drug resistant cell line H460/Gem and its parental cell NCI-H460. *Chin.-Ger. J. Clin. Oncol.* **2008**, *7*, 615−619.
(57) Mahmoodi, N.; Motamed, N.; Paylakhi, S. H. The Comparison of The Effects of Silybin and Silybin-Phosphatidylcholine on Viability and ESR Expression in Human Breast Cancer T47D Cell Line. *Cell J.* **2014**, *16*, 299−308.
(58) Ellig, J.; Fike, R. Regulatory Process, Regulatory Reform, and the Quality of Regulatory Impact Analysis. *J. Benefit-Cost Anal.* **2016**, *7*, 523−559.
(59) Chan, E.; Fucini, R.; Zimmerman, K.; Bui, M.; Hogan, J.; Jackson, M.; Taverna, P.; Howlett, A.; Flanagan, M. 502 POSTER SNS-314, a selective Aurora kinase inhibitor with potent, pre-clinical antitumour activity, shows broad therapeutic potential in combination with standard chemotherapeutics and synergy with microtubule targeted agents. *EJC Suppl.* **2007**, *5*, 90.
(60) Gianni, L.; Dombernowsky, P.; Sledge, G.; Martin, M.; Amadori, D.; Arbuck, S. G.; Ravdin, P.; Brown, M.; Messina, M.; Tuck, D.; Weil, C.; Winograd, B. Cardiac function following combination therapy with paclitaxel and doxorubicin: An analysis of 657 women with advanced breast cancer. *Ann. Oncol.* **2001**, *12*, 1067−1073.
(61) Deng, Z. J.; Morton, S. W.; Ben-Akiva, E.; Dreaden, E. C.; Shopsowitz, K. E.; Hammond, P. T. Layer-by-Layer Nanoparticles for Systemic Codelivery of an Anticancer Drug and siRNA for Potential Triple-Negative Breast Cancer Treatment. *ACS Nano* **2013**, *7*, 9571−9584.
(62) Zhao, Z.; Powers, K.; Hu, Y.; Raleigh, M.; Pentel, P.; Zhang, C. Engineering of a hybrid nanoparticle-based nicotine nanovaccine as a next-generation immunotherapeutic strategy against nicotine addiction: A focus on hapten density. *Biomaterials* **2017**, *123*, 107−117.
(63) Di Martino, A.; Kucharczyk, P.; Capakova, Z.; Humpolicek, P.; Sedlarik, V. Chitosan-based nanocomplexes for simultaneous loading, burst reduction and controlled release of doxorubicin and 5-fluorouracil. *Int. J. Biol. Macromol.* **2017**, *102*, 613−624.
(64) Sun, L.; Chen, Y.; Zhou, Y.; Guo, D.; Fan, Y.; Guo, F.; Zheng, Y.; Chen, W. Preparation of 5-fluorouracil-loaded chitosan nanoparticles and study of the sustained release in vitro and in vivo. *Asian J. Pharm. Sci.* **2017**, *12*, 418−423.
(65) Huang, W.; Zhang, J.; Dorn, H. C.; Geohegan, D.; Zhang, C. Assembly of Single-Walled Carbon Nanohorn Supported Liposome Particles. *Bioconjugate Chem.* **2011**, *22*, 1012−1016.
(66) Kress, J.; Rohrbach, D. J.; Carter, K. A.; Luo, D.; Shao, S.; Lele, S.; Lovell, J. F.; Sunar, U. Quantitative imaging of light-triggered doxorubicin release. *Biomed. Opt. Express* **2015**, *6*, 3546−3555.
(67) Rezazadeh, M.; Emami, J.; Mostafavi, A.; Rostami, M.; Hassanzadeh, F.; Sadeghi, H.; Minaiyan, M.; Lavasanifar, A. A Rapid and Sensitive HPLC Method for Quantitation of Paclitaxel in Biological Samples using Liquid-Liquid Extraction and UV Detection: Application to Pharmacokinetics and Tissues Distribution Study of Paclitaxel Loaded Targeted Polymeric Micelles in Tumor Bearing Mice. *J. Pharm. Pharm. Sci.* **2015**, *18*, 647−660.
(68) Li, W.; Gao, J.; Zhao, H.-Z.; Liu, C.-X. Development of a HPLC-UV assay for silybin-phosphatidylcholine complex (silybinin capsules) and its pharmacokinetic study in healthy male Chinese volunteers. *Eur. J. Drug Metab. Pharmacokinet.* **2006**, *31*, 265−270.
(69) Hu, Y.; Hoerle, R.; Ehrich, M.; Zhang, C. Engineering the lipid layer of lipid-PLGA hybrid nanoparticles for enhanced in vitro cellular uptake and improved stability. *Acta Biomater.* **2015**, *28*, 149−159.
(70) He, Z.; Schulz, A.; Wan, X.; Seitz, J.; Bludau, H.; Alakhova, D. Y.; Darr, D. B.; Perou, C. M.; Jordan, R.; Ojima, I.; Kabanov, A. V.; Luxenhofer, R. Poly(2-oxazoline) based micelles with high capacity for 3rd generation taxoids: preparation, in vitro and in vivo evaluation. *J. Controlled Release* **2015**, *208*, 67−75.
(71) Li, Y.; Yang, J.; Xu, B.; Gao, F.; Wang, W.; Liu, W. Enhanced Therapeutic siRNA to Tumor Cells by a pH-Sensitive Agmatine-Chitosan Bioconjugate. *ACS Appl. Mater. Interfaces* **2015**, *7*, 8114−8124.

DOI: 10.1021/acsomega.8b00949
ACS Omega 2018, 3, 9210−9219